mater.scichina.com link.springer.com

Published online 18 January 2021 | https://doi.org/10.1007/s40843-020-1580-3
Sci China Mater 2021, 64(6): 1378–1385

Interplay between Li_3YX_6 (X = Cl or Br) solid electrolytes and the Li metal anode

Yuanyuan Fu and Cheng Ma*

ABSTRACT **The interplay between solid electrolytes and electrodes is of vital importance to the performance of all-solid-state Li batteries. Recently, halide superionic conductors have emerged as a new family of high-performance solid electrolytes, but their compatibility with Li metal, i.e., the anode with the highest theoretical capacity, has not been systematically studied. Here, we investigate the interaction between Li metal and two representative halide solid electrolytes: Li_3YCl_6 and Li_3YBr_6. Both materials are found to form interphases with Li, similar to most solid electrolytes. However, the interphases observed here contain electronic conducting components, which are detrimental to their compatibility with Li. By elucidating this phenomenon, the present study provides guiding principles for improving the Li compatibility of halide solid electrolytes.**

Keywords: solid electrolytes, Li metal anode, halides, interfacial stability

INTRODUCTION

Compared with present commercial Li-ion batteries, all-solid-state Li batteries (ASSLBs) are safer and may likely exhibit a further improvement in energy density [1–4]. Identifying a solid electrolyte showing conductivity and interfacial properties comparable to those of conventional organic liquid electrolytes is the key to the success of ASSLBs [5].

Recently, halide solid electrolytes with a rare combination of multiple appealing characteristics have been increasingly studied [5–9]. Unlike widely studied oxide and sulfide superionic conductors, these materials can simultaneously possess high ionic conductivity (up to 10^{-3} S cm^{-1}), good deformability, and excellent compatibility with 4 V–class cathodes [5]. This unique advantage leads to excellent cell performance. When Li_3YCl_6 and Li_3YBr_6, i.e., the first two halides reported as solid electrolytes for batteries [8], were integrated with 4 V-class cathodes, the all-solid-state cells exhibited negligible interfacial resistance and excellent Coulombic efficiencies that are above 94%. More importantly, this was achieved without any extra coating that is typically needed for sulfide solid electrolytes. Following the above report on Li_3YCl_6 and Li_3YBr_6 in 2018 [8], researchers discovered similar superior performance in many other halide solid electrolytes, including Li_3InCl_6 [7,9–11], Li_3ScCl_6 [12], and Li_3ErCl_6 [13–15]. Li_3MX_6-type (M = non-Li element, X = Cl or Br) halides have thus rapidly become a popular family of high-performance solid electrolytes [5].

Despite the intensive research interest in Li_3MX_6, the interplay between these halides and Li metal (the anode showing the highest theoretical capacity, i.e., 3860 mA h g^{-1} [16,17]) has not been systematically studied. In the existing literature, Li metal has rarely been contacted directly with Li_3MX_6. In the study reporting on Li_3YCl_6 and Li_3YBr_6, the anode used in the all-solid-state cell was a Li-In alloy instead of Li [8]. All-solid-state cells with Li_3InCl_6 were reported to use the Li metal anode, but Li and the halide are separated by $Li_7P_3S_{11}$ [7]. Only Li_3ScCl_6 [12] and Li_3YBr_6 [18] have been in direct contact with Li in symmetric Li/Li_3MX_6/Li cells, and high overpotentials were observed in both cases. Although this phenomenon, along with the calculated reduction potentials [19,20], seems to suggest their instability with Li, what exactly happens between these two materials, for instance, whether any interphase is formed, what the structure and properties of the interphase are, how the interfacial behaviors are influenced by these characteristics, remain open questions. Without such knowledge, neither interfacial optimization nor material design can occur in a target-oriented manner.

Here, we unravel the interplay between Li and two representative Li_3MX_6 materials: Li_3YCl_6 and Li_3YBr_6.

Division of Nanomaterials & Chemistry, Hefei National Laboratory for Physical Sciences at the Microscale, CAS Key Laboratory of Materials for Energy Conversion, Department of Materials Science and Engineering, University of Science and Technology of China, Hefei 230026, China
* Corresponding author (email: mach16@ustc.edu.cn)

Similar to most solid electrolytes [21], both halides form interphases with Li. However, the interphase between Li_3YX_6 (referred to as LYX below) and Li contains electronic conducting components, which are detrimental to the Li compatibility of solid electrolytes.

EXPERIMENTAL SECTION

Synthesis

Li_3YCl_6 with low crystallinity (lc-LYC) was prepared by milling a mixture of LiCl (Alfa Aesar, 99.90%) and YCl_3 (Alfa Aesar, 99.90%) with a molar ratio of 3:1 in a planetary ball mill at 600 rpm for 20 h. Tungsten carbide pots with Φ 5 mm tungsten carbide balls were used. Li_3YCl_6 with high crystallinity (hc-LYC) was obtained by calcining lc-LYC at 500°C for 5 h. Similarly, Li_3YBr_6 with low crystallinity (lc-LYB) was synthesized by ball milling a mixture of LiBr (Aladdin, 99.90%) and YBr_3 (Aladdin, 99.90%) with a molar ratio of 3:1 at 600 rpm for 60 h. Li_3YBr_6 with high crystallinity (hc-LYB) was obtained by calcining lc-LYB at 550°C for 5 h. During all the above procedures, the samples were never exposed to ambient air.

Characterization

The phase purity of the halide samples was studied by X-ray diffraction (XRD). All the samples were sealed in Kapton films to avoid air exposure during measurement. Diffraction data were collected using a Cu Kα radiation source.

The ionic conductivity of LYX was evaluated by electrochemical impedance spectroscopy (EIS). The measurement was performed on cold-pressed pellets sputtered with gold on their surface; the pellet was obtained by pressing the solid electrolyte powder in a die set with an inner diameter of 10 mm under 300 MPa. EIS was measured in the frequency range between 7 MHz and 10 mHz at an amplitude of 10 mV in an Ar atmosphere.

The interfacial resistance between Li and LYX was also evaluated by EIS. The Li/LYX/Li sandwiches used for this purpose were prepared in an argon-filled glove box. First, 200 mg of LYX powder was cold-pressed under 500 MPa into a pellet with a diameter of 17 mm. Then, two pieces of Li foil with the same diameters were attached on both sides of the pellet under a pressure of 300 MPa. The LYX/Li pellets used to study the reaction products were prepared by the same procedure, except that 400 mg, rather than 200 mg, of LYX was used. After the Li foils on such pellets turned completely black, the pellets were ground into powder for XRD.

The electronic conductivity was determined by a direct-current polarization measurement under an applied voltage of 2 V. In regard to the pristine LYX materials, the electronic conductivity measurement was performed on cold-pressed pellets with Au electrodes sputtered on both sides. For the interphase between LYX and Li, the electronic conductivity was determined on pellets with co-planar electrodes [22,23]. More specifically, LYX was first contacted with Li for 200 h, and then the Li foil was removed using 2000 mesh sandpaper to expose the interphase. Next, two rectangular-shaped Au electrodes that were 2 mm from each other were sputtered on the interphase for the direct-current polarization measurement. The electronic conductivity was calculated from the current *vs.* time curve using Ohm's law: $\sigma = IL/US$, where I is the steady current, L is the distance between the gold electrodes (2 mm), U is the applied voltage (2 V), and S is the sectional area for the charge-carrier migration (equal to the depth of interphase multiplied by the length of the Au electrodes, i.e., 5 mm).

RESULTS AND DISCUSSION

LYX with low crystallinity (lc-LYX) and high crystallinity (hc-LYX) were both investigated in the present study. The materials we used were consistent with those in the literature [8] in terms of both crystal structure (Fig. S1) and ionic conductivity (Fig. S2). The lc-LYX samples were produced directly by a planetary mill without any heat treatment. As a result, they contained a large fraction of the amorphous phase, as characterized by broad diffraction peaks (Fig. S1). In contrast, the hc-LYX samples were acquired by annealing lc-LYX at high temperatures, so the amorphous phase was largely eliminated, and the diffraction peaks were sharp (Fig. S1). The amorphous LYC seemed more conductive than its crystalline counterpart, so lc-LYC, with a higher amorphous phase content, showed a conductivity that was an order of magnitude higher than hc-LYC (Fig. S2). For LYB, the situation was just the opposite: hc-LYB was a lot more conductive than lc-LYB due to the higher conductivity of crystalline LYB (Fig. S2). The detailed mechanism behind this phenomenon is not yet conclusive in the literature [8,15,19]. Regardless, the interplay with Li was investigated for both lc- and hc-LYX in the present study. First, we probed the interfacial resistance between the Li metal and LYX. The Nyquist plots of the Li/LYX/Li sandwiches at different times after assembly are displayed in Fig. S3, and the evolution of their total area specific resistances (ASR) over time is summarized in Fig. 1. The resistances of all the Li/LYX/Li sandwiches increased ra-

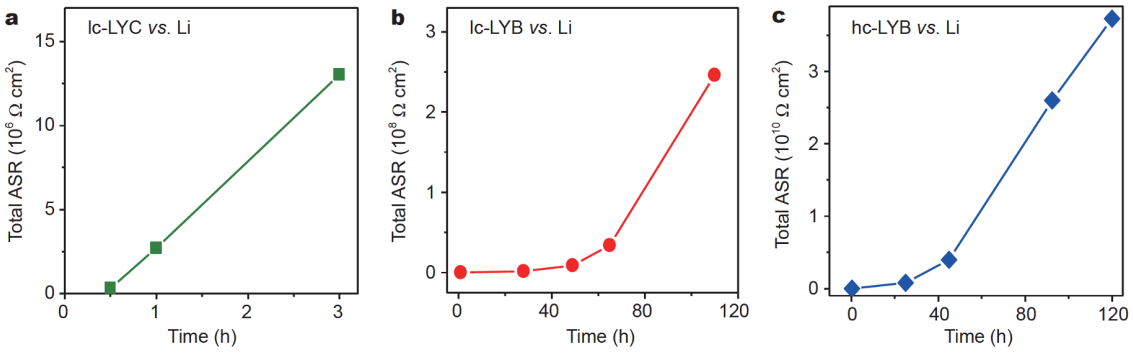

Figure 1 Total ASR of the (a) Li/lc-LYC/Li, (b) Li/lc-LYB/Li, and (c) Li/hc-LYB/Li sandwiches at different times after assembly.

pidly, suggesting that interfacial reactions occurred continuously. The interfacial resistance between hc-LYC and Li increased particularly fast, so that the resistance of the Li/hc-LYC/Li sandwich exceeded the instrument measuring range (500 MΩ) shortly after its assembly, leaving only irregularly scattered data points (Fig. S3b). Eventually, the same happened to all the Li/LYX/Li sandwiches; the only difference was how fast their resistances increased over time (Fig. 1). Based on these observations, all four LYX solid electrolytes studied here must react continuously with Li metal instead of forming a passivation layer through a self-limiting reaction.

In addition to the Nyquist plots, the color of the LYX/Li pellets also suggested that the reactions proceeded continuously. When Li foil was just contacted with LYX, its surface was shiny with a silver color (Fig. 2). As time passed, black spots began to appear on the Li foil. These spots continued to grow in both size and number, and eventually, the entire surface of the Li foil became black. This result suggested that the reaction between LYX and Li would not stop until one of the reactants (in this case Li) was completely consumed. In other words, the reaction was not self-limiting. With the Li foil showing the same thickness in the four LYX/Li pellets in Fig. 2, the time needed to complete the reactions varied with the composition and crystallinity. Materials with high crystallinity generally consumed Li faster. For example, hc-LYC and hc-LYB needed 336 and 582 h, respectively, to complete the reaction. In contrast, lc-LYC and lc-LYB took 740 and 800 h, respectively, to blacken the Li foil. The lower reaction rate of lc-LYX may be attributed to the amorphous or defective regions on the particle surfaces. The reduction potential of such regions might be lower than that of the highly crystalline LYC; consequently, their thermodynamic driving force for Li reduction would be smaller. On the other hand, the data

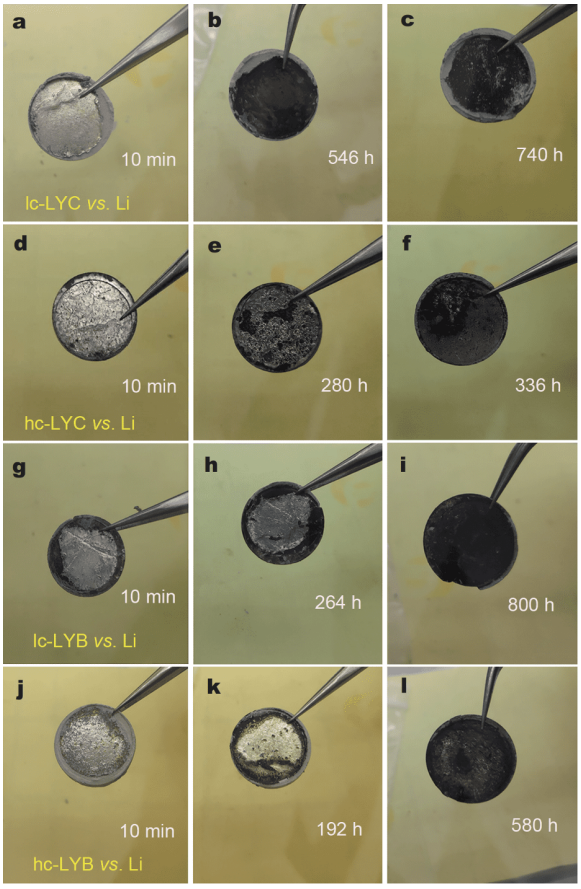

Figure 2 Photographs of LYX/Li pellets at different times after LYX contacts Li: (a–c) lc-LYC/Li, (d–f) hc-LYC/Li, (g–i) lc-LYB/Li, and (j–l) hc-LYB/Li.

above also suggested that the reaction time for LYC was shorter than that for LYB, regardless of the crystallinity. This result may also be correlated with their reduction potentials. LYC is known to possess a slightly higher reduction potential than LYB (0.62 *vs.* 0.59 V) [19], so the

thermodynamic driving force of Li reduction should be higher for LYC, leading to a faster reaction.

To determine why the reactions above proceeded continuously instead of being self-limited, we examined the reaction products. To this end, the LYX/Li pellets in Fig. 2 were ground into powder for XRD when the Li foil turned totally black. According to the XRD results in Fig. 3, LYX (corresponding to the unlabeled peaks) was present in all four LYX/Li pellets. This result was consistent with the fact that Li was completely consumed (turned black), leaving the other reactant, i.e., LYX, remaining in the LYX/Li pellet. The phases other than LYX shown in Fig. 3 were the reaction products between LYX and Li, and their diffraction peaks were all labeled. Li and LYC reacted to form Y and LiCl, regardless of the crystallinity of LYC. Similarly, both lc- and hc-LYB reacted with Li to produce Y and LiBr. It should be noted that the Y produced by reducing LYC showed a different crystal structure from the Y generated by reducing LYB. The former belonged to the $Fm\bar{3}m$ space group, while the latter showed $P6_3/mmc$ symmetry. In addition to these components, no other phases were observed. Generally, the reaction products between LYX and Li should be LiX and Y.

This scenario was further verified by estimating the molar ratio between LiX and Y in the reaction products. Assuming the reduction of LYX by Li yielded LiX and Y, the balanced chemical equations can be written as:

$Li_3YBr_6 + 3Li \rightarrow 6LiBr + Y$,

$Li_3YCl_6 + 3Li \rightarrow 6LiCl + Y$.

Therefore, if the reaction did occur in this way, the molar ratio of LiX:Y should be close to 6. To estimate this ratio, we performed Rietveld refinement for the data in Fig. 3, i.e., the XRD patterns of LYX/Li pellets after the reactions were completed. For all four LYX materials studied here, excellent agreement between the calculated and experimental diffraction patterns was achieved when the data were refined using the coexisting LYX, LiX, and Y phases (Fig. 4). Once again, this result confirmed that only LiX and Y existed in the final reaction products, it also suggested that the refinement quality was acceptable. According to such results, the LiX:Y molar ratios were found to be close to 6 for all four LYX samples (Table 1), consistent with the value indicated by the chemical equations above. These data further confirmed that the reaction between LYX and Li led to the formation of LiX and Y metal.

With the reaction products determined, we can infer the reason why LYX reacted continuously with Li instead of forming a passivation layer at the interface, similar to many other sulfide and oxide solid electrolytes [24]. Ac-

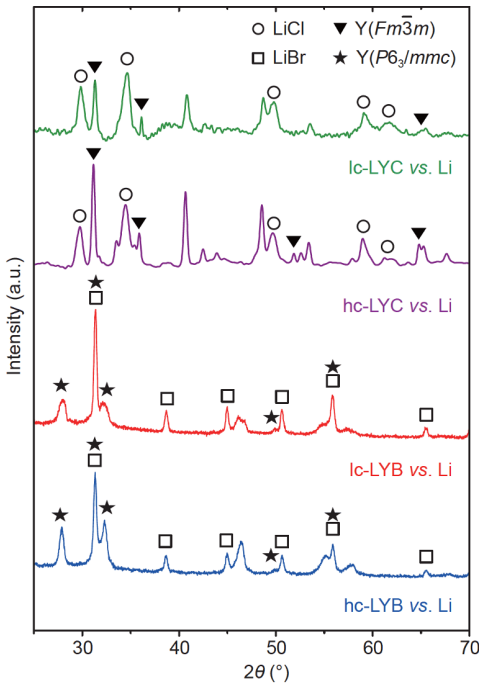

Figure 3 XRD patterns of the products after the reaction of LYB and LYC with Li. All the unlabeled peaks belong to the unreacted LYX.

cording to Zhu *et al.* [25], the interfacial behavior between solid electrolytes and Li may be divided into three types. (1) A thermodynamically stable interface with no decomposition interphase layer [26]. (2) The solid electrolyte will be reduced by Li, forming an interphase consisting of mixed ionic and electronic conductors (MIECs). With this interphase transporting both Li^+ and electrons between the unreacted solid electrolyte and Li, the redox reaction is allowed to proceed continuously [27,28]. (3) The solid electrolyte will be reduced by Li, but the resulting interphase is electronically insulating. As a result, it blocks electron transport and terminates the redox reaction, providing passivation at the interface [29]. According to the reaction products disclosed above, the interfacial behavior between LYX and Li should belong to the second type. Although none of the individual components in the LYX/Li interphase is an MIEC, the interphase contained both the Li-ion-conducting phase and electronic conducting phase. As a result, it was in fact capable of transporting both Li^+ and electrons. The growth process of the interphase is schematically illustrated in Fig. 5. When Li metal and LYX were just in contact with each other, Li^+ and the electrons in Li entered LYX, reducing the interfacial region into Y and LiX (Fig. 5a). As a metal, Y could conduct electrons, while LiX could transport Li ions. In this way, both electrons and

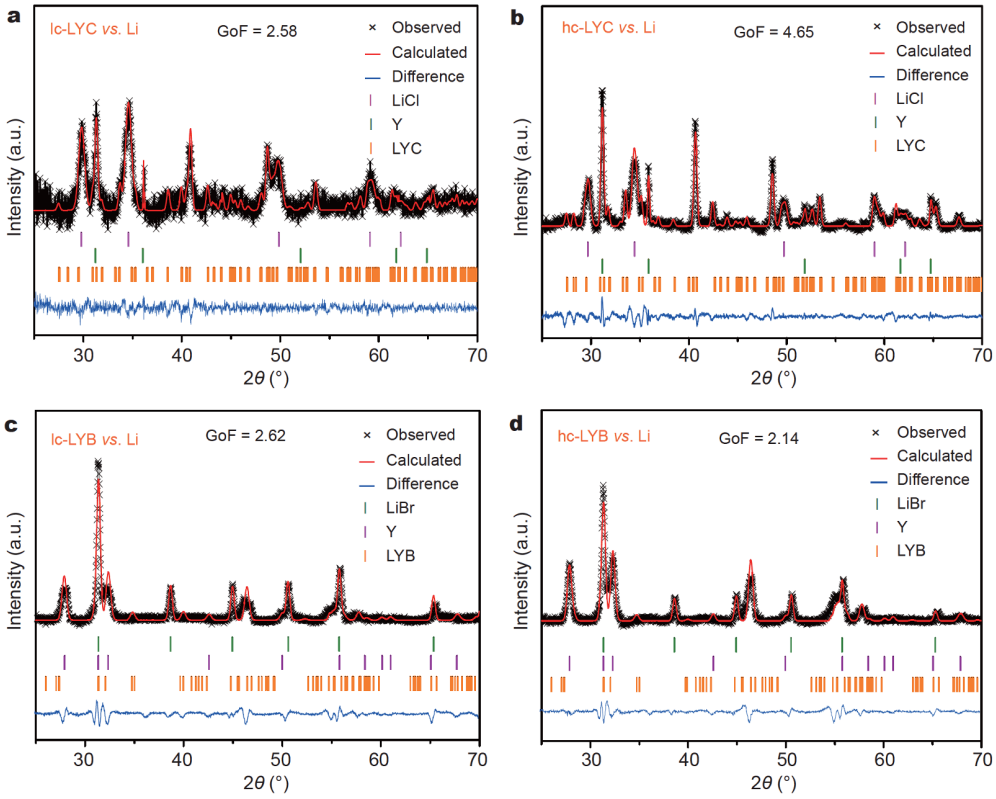

Figure 4 Refined XRD patterns of the powder ground from the LYX/Li pellets after the reactions were complete. (a) lc-LYC/Li, (b) hc-LYC/Li, (c) lc-LYB/Li, (d) hc-LYB/Li. GoF stands for goodness of fit.

Table 1 Weights and molar fractions of each phase obtained by Rietveld refinement of the XRD patterns in Fig. 3

Sample	Observed phases	Weight fraction (%)	Mole fraction (%)
lc-LYC *vs.* Li	LYC	23.76	4.65
	LiCl	55.98	83.25
	Y	20.26	14.37
hc-LYC *vs.* Li	LYC	49.91	13.38
	LiCl	35.96	73.32
	Y	14.13	13.74
lc-LYB *vs.* Li	LYB	82.68	68.68
	LiBr	14.97	27.16
	Y	2.35	4.16
hc-LYB *vs.* Li	LYB	83.75	72.74
	LiBr	14.07	26.68
	Y	2.18	4.04

Li^+ could migrate through the reduced interfacial region into the unreacted material, converting even more LYX into Y and LiX (Fig. 5b). This scenario was supported by the electronic conductivities of the interphases, which were measured using a direct-current polarization method (details described in Fig. S4 and the EXPERIMENTAL SECTION) [22,23]. As shown in Table S1, the electronic conductivity of the interphase was found to be orders of magnitude higher than that of the pristine material for all four LYX samples studied here (10^{-6} *vs.* 10^{-8}–10^{-9} S cm^{-1}), suggesting that the reaction with Li indeed gave rise to considerable electronic conductivity. More importantly, the values of the interphase electronic conductivity correlated very well with the kinetics of the interfacial reaction. As shown in Fig. S5, the halide possessing a more electronically conductive interphase always needed less time to consume Li foils with the same thickness. These corroborating results confirmed that the electronic conductivity of the interphase was responsible for the non-self-limiting nature of the reaction with Li. Beyond the chlorides and bromides studied here, this scenario, i.e., being continuously reduced by Li, may very likely also happen to many fluoride solid electrolytes. According to calculations performed by Wang *et al.* [19], quite a few fluoride solid electrolytes show reduction

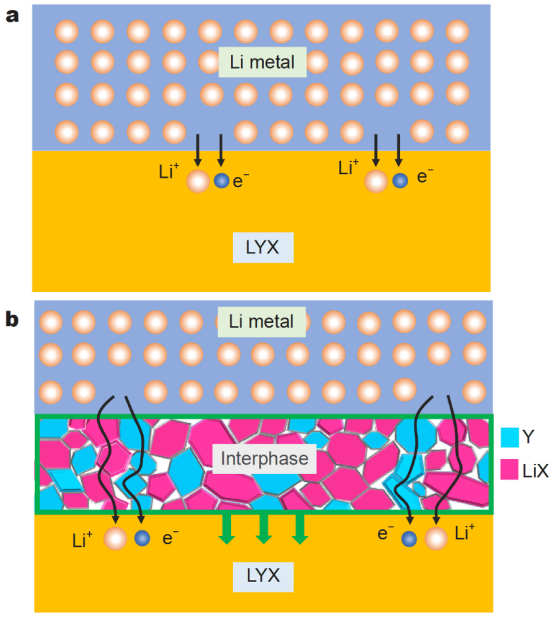

Figure 5 Schematic illustrations showing the interplay between Li and LYX. (a) When LYX just contacts Li metal, it is reduced, i.e., receives electrons (along with Li ions) in the interfacial region. (b) This process forms an interphase containing Y and LiX that can conduct electrons and ions, respectively. Such an interphase can keep transporting Li^+ and electrons from Li to the unreacted LYX so that the reduction proceeds continuously.

potentials above 0 V, while the reduction products contain LiF (Li-ion conducting) and a metal (electron conducting). Therefore, the interphase was still an MIEC that could grow continuously. It should be noted that the damage caused by the continuous reaction with Li might not be limited to the degradation of the solid electrolyte itself. The significant, violent volume variation associated with the continuous decomposition of LYX into Y and LiX would very likely produce large amounts of stress, eventually compromising the contact between the solid electrolyte and Li. Similar phenomena have also been observed in many other solid electrolytes [21,22,30].

Considering that the decomposition products of nearly all the solid electrolytes contain Li-ion-conducting components [31], whether the interphase would become an MIEC (and thus could continuously grow) depends on whether it contains the electronic conducting component. According to the results here, this effect seems even more important than the reduction potential when evaluating the "practical" Li compatibility of solid electrolytes. The reduction potential suggests that sulfide solid electrolytes, such as $Li_7P_3S_{11}$ (2.28 V) and Li_6PS_5Cl (1.71 V) [31], are much less stable against Li reduction than Li_3YCl_6 (0.62 V) and Li_3YBr_6 (0.59 V) [19]. Nevertheless, unlike LYX, both $Li_7P_3S_{11}$ and Li_6PS_5Cl will only be reduced to several electronically insulating phases [32]. Since their interphase with Li cannot transport more electrons into the unreacted solid electrolyte, the redox reaction cannot proceed further. Consequently, in practice, these sulfide solid electrolytes can be integrated with Li metal. In contrast, the LYX with much lower reduction potentials cannot, as the electronically conductive Y in the interphase allows the reduction by Li to proceed continuously. Following this logic, the key to designing Li-compatible halide solid electrolytes appears to lie in the selection of the non-Li cation. When the solid electrolyte contacts Li, this cation must not be reduced directly to metal. Instead, its reduction needs to result in an electronically insulating product so that the unreacted solid electrolyte stops receiving electrons. Based on this criterion, nonmetal elements seem to be good candidates. In addition, transition-metal cations with multiple stable, nonzero oxidation states might also be worth consideration; if the reduction of solid electrolytes containing such transition-metal elements only leads to several electronically insulating metal chlorides, instead of metal, the resulting interphase may still serve as a passivation layer that prevents further reactions. In addition to improving the stability of the materials themselves, separating the halides and Li using another solid electrolyte is also a viable strategy. The in-between solid electrolyte must be compatible with Li, while its oxidation potential only needs to be no lower than the reduction potential of the halides. Since the latter is not very high (0.62 and 0.59 V for LYC and LYB, respectively), many solid electrolytes are promising candidates, including Li_3OCl [33], $0.7Li(CB_9H_{10})$–$0.3Li(CB_{11}H_{12})$ [34], and $Li_{10}P_3S_{12}I$ [35].

CONCLUSIONS

In summary, we investigate the interplay between Li metal and LYX solid electrolytes with different crystallinities. These halides form interphases with Li, similar to most sulfide and oxide solid electrolytes. However, the interphase between halides and Li will not stop growing until either Li or the solid electrolyte is consumed. Such behavior is mainly attributed to the presence of Y^{3+} in the halides. When LYX contacts Li, Y^{3+} is reduced directly to Y metal. With this electronic conductor present in the interphase between LYX and Li, LYX can receive not only Li ions but also electrons from the Li metal, regardless of how thick the interphase layer becomes. As a result, the redox reaction keeps occurring. To make improvements, future material design should avoid the inclusion of cations that can be easily reduced to metal. By elucidating

the interplay between LYX and Li metal, the present study provides guidelines for developing Li-compatible halide solid electrolytes.

Received 31 August 2020; accepted 26 November 2020; published online 18 January 2021

1 Goodenough JB, Park KS. The Li-ion rechargeable battery: a perspective. J Am Chem Soc, 2013, 135: 1167–1176
2 Janek J, Zeier WG. A solid future for battery development. Nat Energy, 2016, 1: 16141
3 Famprikis T, Canepa P, Dawson JA, *et al.* Fundamentals of inorganic solid-state electrolytes for batteries. Nat Mater, 2019, 18: 1278–1291
4 Manthiram A, Yu X, Wang S. Lithium battery chemistries enabled by solid-state electrolytes. Nat Rev Mater, 2017, 2: 105–126
5 Li X, Liang J, Yang X, *et al.* Progress and perspectives on halide lithium conductors for all-solid-state lithium batteries. Energy Environ Sci, 2020, 13: 1429–1461
6 Zhou L, Kwok CY, Shyamsunder A, *et al.* A new halospinel superionic conductor for high-voltage all solid state lithium batteries. Energy Environ Sci, 2020, 13: 2056–2063
7 Li X, Liang J, Luo J, *et al.* Air-stable Li_3InCl_6 electrolyte with high voltage compatibility for all-solid-state batteries. Energy Environ Sci, 2019, 12: 2665–2671
8 Asano T, Sakai A, Ouchi S, *et al.* Solid halide electrolytes with high lithium-ion conductivity for application in 4 V class bulk-type all-solid-state batteries. Adv Mater, 2018, 30: 1803075
9 Li X, Liang J, Chen N, *et al.* Water-mediated synthesis of a superionic halide solid electrolyte. Angew Chem Int Ed, 2019, 58: 16427–16432
10 Li X, Liang J, Adair KR, *et al.* Origin of superionic $Li_3Y_{1-x}In_xCl_6$ halide solid electrolytes with high humidity tolerance. Nano Lett, 2020, 20: 4384–4392
11 Tomita Y, Matsushita H, Kobayashi K, *et al.* Substitution effect of ionic conductivity in lithium ion conductor, $Li_3InBr_{6-x}Cl_x$. Solid State Ion, 2008, 179: 867–870
12 Liang J, Li X, Wang S, *et al.* Site-occupation-tuned superionic Li_xScCl_{3+x} halide solid electrolytes for all-solid-state batteries. J Am Chem Soc, 2020, 142: 7012–7022
13 Muy S, Voss J, Schlem R, *et al.* High-throughput screening of solid-state Li-ion conductors using lattice-dynamics descriptors. iScience, 2019, 16: 270–282
14 Park KH, Kaup K, Assoud A, *et al.* High-voltage superionic halide solid electrolytes for all-solid-state Li-Ion batteries. ACS Energy Lett, 2020, 5: 533–539
15 Schlem R, Muy S, Prinz N, *et al.* Mechanochemical synthesis: A tool to tune cation site disorder and ionic transport properties of Li_3MCl_6 (M = Y, Er) superionic conductors. Adv Energy Mater, 2019, 10: 1903719
16 Xu W, Wang J, Ding F, *et al.* Lithium metal anodes for rechargeable batteries. Energy Environ Sci, 2014, 7: 513–537
17 Kim H, Jeong G, Kim YU, *et al.* Metallic anodes for next generation secondary batteries. Chem Soc Rev, 2013, 42: 9011–9034
18 Yu C, Li Y, Adair KR, *et al.* Tuning ionic conductivity and electrode compatibility of Li_3YBr_6 for high-performance all solid-state Li batteries. Nano Energy, 2020, 77: 105097
19 Wang S, Bai Q, Nolan AM, *et al.* Lithium chlorides and bromides as promising solid-state chemistries for fast ion conductors with good electrochemical stability. Angew Chem Int Ed, 2019, 58: 8039–8043
20 Zhu Y, Mo Y. Materials design principles for air-stable lithium/sodium solid electrolytes. Angew Chem Int Ed, 2020, 59: 17472–17476
21 Lewis JA, Cortes FJQ, Boebinger MG, *et al.* Interphase morphology between a solid-state electrolyte and lithium controls cell failure. ACS Energy Lett, 2019, 4: 591–599
22 Zhu J, Zhao J, Xiang Y, *et al.* Chemomechanical failure mechanism study in NASICON-type $Li_{1.3}Al_{0.3}Ti_{1.7}(PO_4)_3$ solid-state lithium batteries. Chem Mater, 2020, 32: 4998–5008
23 Hartmann P, Leichtweiss T, Busche MR, *et al.* Degradation of NASICON-type materials in contact with lithium metal: formation of mixed conducting interphases (MCI) on solid electrolytes. J Phys Chem C, 2013, 117: 21064–21074
24 Chen R, Li Q, Yu X, *et al.* Approaching practically accessible solid-state batteries: stability issues related to solid electrolytes and interfaces. Chem Rev, 2020, 120: 6820–6877
25 Zhu Y, He X, Mo Y. First principles study on electrochemical and chemical stability of solid electrolyte–electrode interfaces in all-solid-state Li-ion batteries. J Mater Chem A, 2016, 4: 3253–3266
26 Murugan R, Thangadurai V, Weppner W. Fast lithium ion conduction in garnet-type $Li_7La_3Zr_2O_{12}$. Angew Chem Int Ed, 2007, 46: 7778–7781
27 Han F, Gao T, Zhu Y, *et al.* A battery made from a single material. Adv Mater, 2015, 27: 3473–3483
28 Chen C. Ionic conductivity, lithium insertion and extraction of lanthanum lithium titanate. Solid State Ion, 2001, 144: 51–57
29 Schwöbel A, Hausbrand R, Jaegermann W. Interface reactions between LiPON and lithium studied by *in-situ* X-ray photoemission. Solid State Ion, 2015, 273: 51–54
30 Tippens J, Miers JC, Afshar A, *et al.* Visualizing chemomechanical degradation of a solid-state battery electrolyte. ACS Energy Lett, 2019, 4: 1475–1483
31 Zhu Y, He X, Mo Y. Origin of outstanding stability in the lithium solid electrolyte materials: insights from thermodynamic analyses based on first-principles calculations. ACS Appl Mater Interfaces, 2015, 7: 23685–23693
32 Wenzel S, Sedlmaier SJ, Dietrich C, *et al.* Interfacial reactivity and interphase growth of argyrodite solid electrolytes at lithium metal electrodes. Solid State Ion, 2018, 318: 102–112
33 Lü X, Wu G, Howard JW, *et al.* Li-rich anti-perovskite Li_3OCl films with enhanced ionic conductivity. Chem Commun, 2014, 50: 11520–11522
34 Kim S, Oguchi H, Toyama N, *et al.* A complex hydride lithium superionic conductor for high-energy-density all-solid-state lithium metal batteries. Nat Commun, 2019, 10: 1081
35 Feng X, Chien PH, Patel S, *et al.* Synthesis and characterizations of highly conductive and stable electrolyte $Li_{10}P_3S_{12}I$. Energy Storage Mater, 2019, 22: 397–401

Acknowledgements This research was supported by the National Key R&D Program of China (2018YFA0209600 and 2017YFA0208300), the National Natural Science Foundation of China (51802302), and the Fundamental Research Funds for the Central Universities (WK3430000006).

Author contributions Fu Y conducted the experiments and wrote the manuscript. Ma C provided the overall concept and supervised the research.

Conflict of interest The authors declare that they have no conflicts of interest.

Supplementary information Experimental details and supporting data are available in the online version of the paper.

Yuanyuan Fu received her Bachelor's degree from Nanjing University of Science and Technology in 2018 and is currently studying for her Master's degree at the University of Science and Technology of China (USTC). Her main research interests focus on all-solid-state batteries and halide solid state electrolytes.

Cheng Ma received his BS degree of materials science and engineering in 2006 from Tsinghua University (Beijing, China) and PhD degree of materials science and engineering in 2012 from Iowa State University. After completing his work as a postdoctoral researcher at the Oak Ridge National Laboratory in 2016, he joined USTC as a professor. His research interest lies in the critical materials and interfaces in all-solid-state Li batteries.

Li_3YX_6(X = Cl或Br)固态电解质和锂金属负极之间的相互作用

符媛媛, 马骋*

摘要 固态电解质与电极之间的相互作用对全固态锂电池的性能至关重要. 最近, 研究者发现了一类新的高性能固态电解质: 卤化物超离子导体. 但是, 它们与锂金属这一理论比容量最高的负极的相容性尚未被系统研究. 本文中, 我们研究了锂金属和两种代表性卤化物固态电解质—Li_3YCl_6和Li_3YBr_6—之间的相互作用. 这两种材料和其他很多固态电解质类似, 与锂发生反应形成中间相. 然而, 此处观察到的中间相包含电子导电成分, 会损害固态电解质对金属锂的相容性. 通过解析这一现象, 本工作为改善金属锂和卤化物固态电解质的相容性提供了指导法则.